Proc. Natl. Acad. Sci. USA
Vol. 93, pp. 4799–4803, May 1996
Cell Biology

High resolution ultrastructural mapping of total calcium: Electron spectroscopic imaging/electron energy loss spectroscopy analysis of a physically/chemically processed nerve–muscle preparation

(mitochondria/sarcoplasmic reticulum/smooth endoplasmic reticulum/synaptic vesicles)

FABIO GROHOVAZ*, MARIO BOSSI, ROBERTA PEZZATI, JACOPO MELDOLESI, AND FRANCESCA TORRI TARELLI

"Consiglio Nazionale delle Ricerche," Cellular and Molecular Pharmacology Center, "B. Ceccarelli" Center, Department of Pharmacology, University of Milan, and DIBIT, S. Raffaele Scientific Institute, via Olgettina 58, 20132 Milan, Italy

Communicated by George E. Palade, University of California at San Diego, La Jolla, CA, January 5, 1996 (received for review December 1994)

ABSTRACT **We report on a procedure for tissue preparation that combines thoroughly controlled physical and chemical treatments: quick-freezing and freeze-drying followed by fixation with OsO_4 vapors and embedding by direct resin infiltration. Specimens of frog cutaneous pectoris muscle thus prepared were analyzed for total calcium using electron spectroscopic imaging/electron energy loss spectroscopy (ESI/EELS) approach. The preservation of the ultrastructure was excellent, with positive K/Na ratios revealed in the fibers by x-ray microanalysis. Clear, high-resolution EELS/ESI calcium signals were recorded from the lumen of terminal cisternae of the sarcoplasmic reticulum but not from longitudinal cisternae, as expected from previous studies carried out with different techniques. In many mitochondria, calcium was below detection whereas in others it was appreciable although at variable level. Within the motor nerve terminals, synaptic vesicles as well as some cisternae of the smooth endoplasmic reticulum yielded positive signals at variance with mitochondria, that were most often below detection. Taken as a whole, the present study reveals the potential of our experimental approach to map with high spatial resolution the total calcium within individual intracellular organelles identified by their established ultrastructure, but only where the element is present at high levels.**

The homeostasis of calcium within eukaryotic cells is the result of complex equilibria among multiple pools located in the cytosol as well as within the nucleus and various organelles, where the element is known to play roles of fundamental importance (1). The development of fluorescent indicators (2, 3) together with videoimaging techniques, and the use of recombinant photoproteins (4, 5), have recently provided powerful tools for the dynamic investigation of the fraction of these pools that is in the free, ionized Ca^{2+} state. In contrast, information about the distribution of total calcium in identified subcellular compartments is still fragmentary, due primarily to limitations of analytical electron microscopy techniques and/or inadequacy of preparative procedures for the maintenance in the specimens of the original element distribution (1, 6–11). So far conclusive results have been obtained only by the use of cryosections analyzed by electron probe x-ray microanalysis (EPMA) (7, 8, 12). However, even the latter approach requires the use of relatively thick, unstained preparations. Therefore, solid data have been obtained mainly on large or geometrically distributed structures: nuclei, mitochondria, clusters of vesicles or cisternae, or sarcoplasmic reticulum (SR) (6, 13–18).

An alternative approach that can offer advantages in terms of spatial resolution and organelle identification is electron energy loss microanalysis (19–23), employed in the spectrum mode (electron energy loss spectroscopy; EELS) and/or in the image mode (electron spectroscopic imaging; ESI). With this technique, however, the need to use very thin specimens has represented a severe limitation. As a consequence, until now only a few attempts were made to perform microanalyses on samples where diffusion of the element had been minimized. In particular, the use of cryosections proved problematical, because computational analyses of spectra from multiple areas were necessary to sort out results (24), which turned out to be averages rather than maps of calcium in individual cells. Most other studies were carried out on samples conventionally fixed and embedded in resin, where calcium was identified in precipitates generated by treatment with various anions (see, for example, refs. 25–29). The latter approach is open to serious question. In fact, both theoretical considerations and experimental results indicate that, especially during exposure to aqueous fixatives and dehydration solutions, loss and/or redistribution of calcium from the original location take place (9, 10, 26).

In the present work, physical and chemical steps—quick-freezing, freeze-drying, fixation with OsO_4 vapors, and direct resin infiltration—were combined to preserve both the ultrastructural organization (30) and the elemental distribution of living cells in the preparations to be analyzed by EELS/ESI. The results, obtained in the cutaneous pectoris muscle of the frog, indicate that high-resolution mapping of total calcium is possible by this technique, but only in organelles that are very rich in the element. This conclusion may encourage further use of the approach in different experimental conditions and in other cell systems.

MATERIALS AND METHODS

Specimen Preparation. Cutaneous pectoris muscles from frogs, *Rana pipiens*, were soaked in a Ringer solution (116 mM Na^+/2.1 mM K^+/1.8 mM Ca^{2+}/116 mM Cl^-/6 mM Tris·HCl, pH 7.0; reagents from Merck). After 20-30 min of incubation with 10^{-4} M D-tubocurarine, the muscles were quick-frozen against a liquid helium-cooled copper block (31), transferred to an ultra high vacuum chamber (Cryofract 190; Reichert–Jung), and freeze-dried under controlled conditions. The initial temperature (approximately −150°C) was raised slowly enough to maintain the water partial pressure in the 10^{-8}–10^{-9} Torr range, as monitored by a quadrupole mass spectrometer (Anavac 2; VG Gas Analysis, Winsford, U.K.). At the end of the drying cycle (3–4 days), when room temperature was

The publication costs of this article were defrayed in part by page charge payment. This article must therefore be hereby marked "*advertisement*" in accordance with 18 U.S.C. §1734 solely to indicate this fact.

Abbreviations: EPMA, electron probe x-ray microanalysis; SR, sarcoplasmic reticulum; EELS, electron energy loss spectroscopy; ESI, electron spectroscopic imaging; EM, electron microscope.

*To whom reprint requests should be addressed at: Laboratory of Cellular Neurophysiology, DIBIT, S. Raffaele Scientific Institute, Via Olgettina, 58, 20132 Milan, Italy.

reached, the specimen (thereafter maintained under dry N_2) was removed from the vacuum apparatus, exposed to OsO_4 vapors, and embedded in resin directly (i.e., without conventional dehydration). Among various resins investigated, araldite (Fluka) yielded best results and was thus employed for all the experiments here presented.

Semithin (1 μm) and ultrathin sections were cut with a Reichert–Jung Ultracut microtome and collected on uncoated grids within 15 s of floatation on water. The first sections were used for EPMA, whereas the second sections were examined in a Zeiss CEM 902 electron microscope (EM) by either conventional transmission after staining with uranyl acetate and lead citrate or by ESI and EELS while still unstained.

Electron Probe X-Ray Microanalysis. EPMA elemental analyses were carried out on a Philips EM400T microscope equipped with a tungsten filament operated at 100 KV and interfaced with a 10-mm^2 Si(Li) energy dispersive detector and an EDAX 9100 multichannel analyzer (Edax, Mahwah, NJ). Spectra were obtained with large diameter probes from 1-μm-thick sections mounted on 200-mesh Ni grids. Comparison among different fibers was made by carrying out the analyses with an identical spot diameter, equal current, and for the same time. Data were collected and stored on floppy disks until required for final processing. Inasmuch as the analyses were carried out on OsO_4-fixed, resin-embedded samples, precise quantitation of the various peaks and of their ratios could not be obtained.

Electron Spectroscopic Imaging Analysis. The ultrathin (15-25 nm, gray-tone) sections analyzed by ESI were first examined at 240 eV (i.e. at an energy loss where scattered electrons of most elements contribute to the image), thus providing a general view of the ultrastructural organization (20). The patterns of net calcium distribution were then obtained by computer-assisted processing of two images collected below (330 and 340 eV) and one beyond the calcium-$L_{2,3}$ absorption edge at 350 eV (20). The typical energy width of the imaging electrons was $\approx$5 eV. Each image was the average of 200 frames corrected for nonuniformity with a defocused image collected at the same energy loss (28).

A threshold of calcium values was routinely set to exclude random noise from the final representation. The map thus obtained, represented according to a pseudocolor scale (from dark red to yellow), was superimposed to the corresponding 240-eV image. The nature of calcium signals in the maps was confirmed by EELS spectra.

RESULTS

Ultrastructural and Ionic Preservation of Samples. Fig. 1*A* shows a conventional transmission EM image that illustrates the preservation achieved in the uppermost superficial layer (<10 μm in depth) of muscle fibers prepared according to the procedure of quick-freezing, freeze-drying, OsO_4 vapor fixation, and direct resin infiltration. Compared to samples processed by either conventional techniques or quick-freezing followed by cryosubstitution (31, 32), the organelles, especially mitochondria and synaptic vesicles, appear much more dense and compact, suggesting retention of cell components otherwise extracted during sample processing. The contractile apparatus surrounded by condensed mitochondria and SR cisternae (33, 34) appears adequately preserved. Nerve terminals exhibited mitochondria, elements of the smooth endoplasmic reticulum, and large numbers of synaptic vesicles. The excellent preservation of the structures in the uppermost superficial layers progressively faded out in deeper regions of the quick-frozen specimens, where myofibrils were more and more disorganized by the growth of ice crystals of increasing size (see ref. 31).

EPMA analysis of semithin sections (1 μm) was carried out in muscle fibers such as those of Fig. 1*A* from the impact surface to the deep areas to reveal the balance between K and Na as a marker of the ionic conditions of fibers. The spectrum of Fig. 1*B* shows that in the region underneath the surface the K peak is high and discrete, whereas the Na peak is distinctly lower. Because of the presence in the samples of both the resin and Os, Na peaks are understimated so that K/Na ratios cannot be precisely established (12, 35). However, even when data were normalized to account for these limitations, our results indicate that in the most superficial layers of the fibers K was higher than Na.

At variance with the superficial layers, in deeper regions the fine ultrastructure of muscle preparations was clearly perturbed and the Na peak revealed by EPMA was more prominent (not shown). This result is not surprising because the slowing down of the heat transfer during freezing is known to induce the formation of ice crystals of progressively increasing size (36). We conclude that excellent preservation of ultrastructure is accompanied by the preservation of ionic balance, although in some experimental conditions ionic maintainance was reported to be more critical (37).

Total Calcium ESI Microanalysis. ESI microanalysis was carried out exclusively on the most superficial layers of frozen fibers. Only the thinnest tissue sections, selected on the basis of their gray tone, were examined. Conventional EM images of *en face*-oriented little folds (Fig. 2*C*; see ref. 38) revealed the thickness of these sections to range from 15 to 25 nm (22 $\pm$ 2.1, n = 35). In Figs. 2-4, pairs are presented where the image to the left illustrates the subcellular organization at 240 eV and that to the right shows the same image with the addition of the

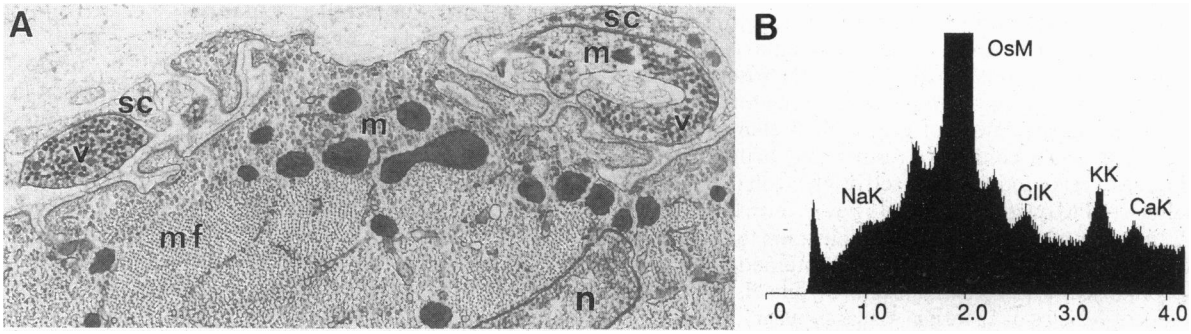

FIG. 1. Conventional EM micrograph and EPMA elemental spectrum of preparations processed by the quick-freezing, freeze-drying, OsO_4 vapor fixation, araldite embedding procedure. (*A*) Typical organization of a muscle fiber as revealed after staining with uranyl acetate and lead citrate. In the most superficial layer, excellent preservation is documented by the various structures in the fiber: orderly arranged myofilaments (mf), dense mitochondria (m), and the nucleus (n). The nerve terminals surrounded by Schwann cells (sc) exhibit mitochondria (m) and a large number of synaptic vesicles (v). (×18,000.) (*B*) The EPMA elemental spectrum was obtained from a semithin (1 μm) section from the superficial layer of a sample such as that in *A* that, however, was left unstained. The central peak is that given by Os and the others (labeled from left to right) are given by Na, Cl, K, and Ca. Numbers in abscissa indicate energies expressed in KeV.

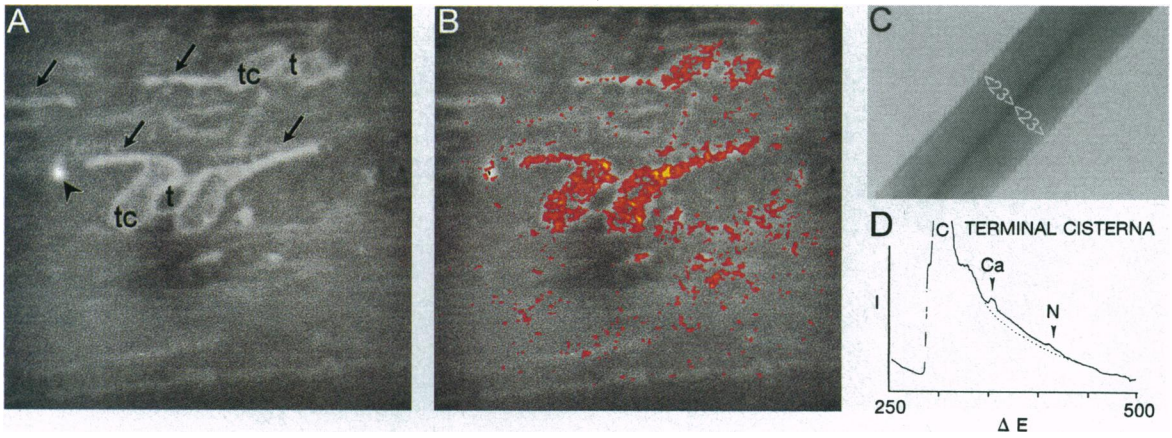

FIG. 2. Calcium distribution in a muscle fiber. (*A*) Subcellular organization of a field as revealed by ESI at 240 eV. (*B*) The same image as in *A* plus the addition of the superimposed net calcium map represented by pseudocolors, ranging from dark red to yellow (low to high calcium content). Two triads are shown to contain elevated amounts of calcium concentrated within the terminal cisternae (tc) while the transverse tubules (t) and the SR longitudinal cisternae (arrows) appear poor or negative. Note that calcium positivity does not correlate with the electron density of organelles as clearly indicated by the low signal in various dense structures including the bright spot indicated by the arrowhead. (×40,500). (*C*) Procedure used to evaluate the thickness of sections used for ESI, based on the measurement of little folds appearing in the analyzed field (in this case, 2 × 23 nm of thickness). (*D*) EELS spectrum recorded from one of the terminal cisternae, confirming the presence of calcium.

superimposed ESI calcium distribution image coded from dark red to yellow (low to high values, respectively). At 240 eV (i.e., below the carbon K-edge), contrast is reversed with respect to conventional bright field images, and thus structures appear white while the cytosol, and even more the extracellular space, look dark (see *A* in Figs. 2–4).

The ESI/EELS analysis of muscle fibers revealed the highest calcium signals within the SR terminal cisternae, recognized by their apposition to triad T tubules (ref. 33; Figs. 2 and 3), whereas in longitudinal cisternae the signal was close or below detection already at short distance from the triads (Fig. 2*B*). At the EELS, clear calcium peaks (Ca-$L_{2,3}$ edge) appeared in the terminal cisternae spectra together with the prominent carbon (C-K edge) and nitrogen signals (N-K edge) (Fig. 2*D*). Spectra were highly reproducible as documented by measurements repeated up to 30-fold in the same area, in which calcium and carbon peaks varied in size less than 10%, indicating that mass loss during individual measurements was negligible. Mitochondria that, in agreement with the transmission EM data (Fig. 1*A*), exhibited a dense homogeneous appearance obscuring appreciation of membranes and cristae were often localized close to the triads. In the mitochondrial populations, many failed to exhibited any detectable calcium signal (not shown), whereas a fraction, even in the same fiber, appeared variably positive (Fig. 3). In all cases, however, mitochondria were less positive for calcium than the SR terminal cisternae. No EELS signal was appreciated in cytosolic areas. When sections, before analysis by ESI/EELS, were soaked for 30 min in water containing 1 mM EGTA, calcium signals were no longer detected in muscle fibers (not shown).

Neuromuscular junctions were also analyzed (Fig. 4). Consistent ESI/EELS signals were observed in the vast majority of synaptic vesicles whether they were located close to or some distance from the active zones (Fig. 4*B*) and also in some cisternal structures identified as elements of the smooth endoplasmic reticulum. Within mitochondria the signal was most often absent; in a few cases it was variable and irregularly distributed (Fig. 4*B*). Also, in the nerve terminal the calcium nature of ESI signals was confirmed by EELS analyses (Fig. 4 *C* and *D*).

DISCUSSION

Analytical electron microscopy represents the only approach by which mapping of elements can be assessed within the cell. Until now these maps were obtained primarily by EPMA using scanning probes that collect x-rays inside the transmission EM (7, 8, 12). In these studies, the use of cryosections is certainly advantageous, provided that freezing is quick enough to keep crystal size, and thus redistribution of solutes, below the spatial resolution of the elemental analysis (6, 37). Due to the physical basis of EPMA, thinner sections produce higher spatial resolution, but with lower detection sensitivity. In practice, the best assays (spatial resolution ≈100 nm) have been carried out on 100- to 200-nm thick, freeze-dried cryosections, cut from quick-frozen samples (6). Most often, thicker sections were employed (up to 1 μm), with higher elemental sensitivity but lower spatial resolution, which is appropriate only for large structures inside the cell.

ESI/EELS can reveal selected elements with high sensitivity and spatial resolution (19–23), but only when sections are

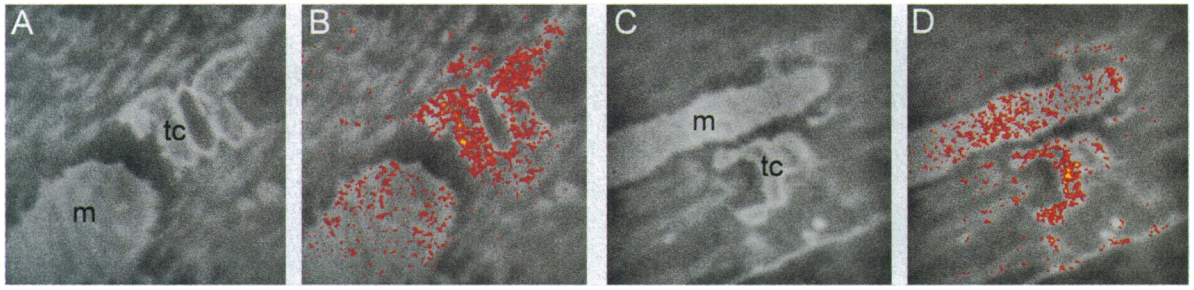

FIG. 3. Calcium maps in other muscle fibers. In the two pairs of images, the calcium map appears on the right. The terminal cisternae (tc) of the two triads exhibit strong calcium signal within their lumen similar to that of Fig. 2*B*. Within two adjacent mitochondria (m) a calcium signal is appreciable, although much lower, especially in the areas apposed to the triads. (×30,800.)

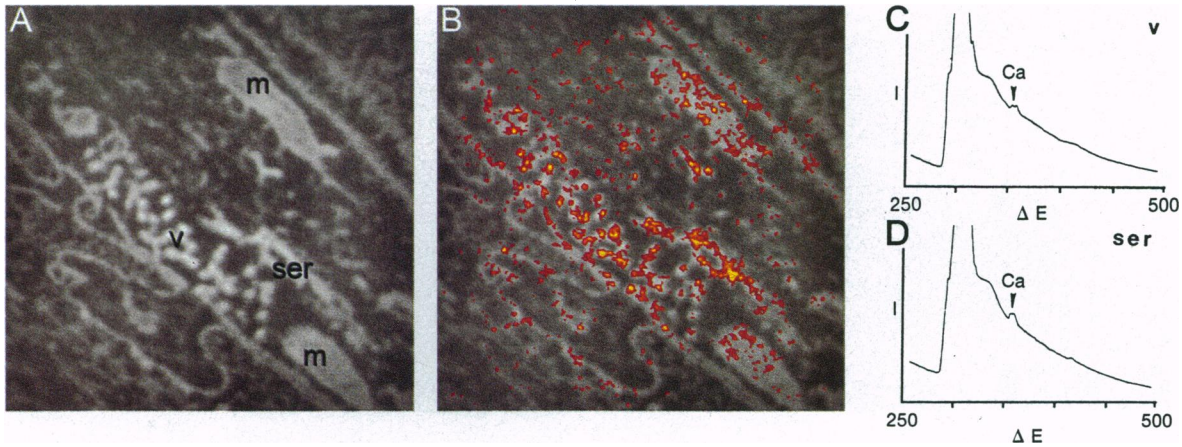

FIG. 4. Calcium distribution and EELS spectra from a motor nerve terminal. Note in *B* that all synaptic vesicles (v) appear rich in calcium, and the same occurs with the lumen of the smooth endoplasmic reticulum cisterna (ser). Also mitochondria (m) appear positive; however, their average calcium signal is distinctly lower and the distribution irregular. (×28,900.) The calcium nature of the ESI map is confirmed by EELS spectra recorded from a cluster of eight synaptic vesicles (*C*) and the SER (*D*).

substantially thinner than the mean free path of inelastic collisions, so that single electrons predominate over multiple scattered electrons, and thus specific signals over background (19, 21, 23, 39). This implies that, at 85-100 KV, only sections thinner than ≈25 nm can be profitably used. This makes the use of cryosections problematical (see ref. 24 and the Introduction). Although the use of ESI instrumentation with higher accelerating voltage should, in principle, allow the use of thicker sections, this approach has not been widely exploited yet. On the other hand, conventional sample preparations appear inadequate for ESI analyses since aqueous fixatives and dehydration solutions are known to induce migration and/or loss of diffusible elements from the original sites of location within the cell. Also, attempts to preserve the native distribution of calcium by addition to fixatives of either the cation itself or calcium precipitating anions are open to serious question inasmuch as artefactual accumulations and/or displacements before the element is ultimately immobilized cannot be excluded (9, 10). Another aspect to be considered is sensitivity. Although in absolute terms the elemental detection is higher for ESI/EELS than EPMA because of the requested thinness of the analyzed specimens and the large contribution of the carbon peak, only relatively high calcium levels can be detected. While the detection sensitivity of EELS has been analyzed in nonbiological standards (21, 40), in cellular samples it has not been precisely established yet. In standards obtained by deposition or evaporation of calcium on different substrates, directly appreciable signals were recorded from samples containing 100 mmol/liter and above calcium (R. Door, personal communication).

To investigate the potential of ESI for calcium mapping in biological specimens, we developed a sample preparation procedure based on the combination of physical and chemical steps: quick-freezing and freeze-drying followed by fixation with OsO_4 vapors and embedding in 100% araldite. A similar approach had been previously proposed by Livesey *et al.* (30) to be used for experimental tasks other than elemental analysis. Two aspects of our procedure are worth emphasizing. First, freeze-drying was performed at temperatures that exclude recrystallization of physiological solutions (30); second, the specimens were never exposed to polar solutions or moisture before embedding. Also important was the precaution to minimize the time (<15 sec) the sections remained in contact with water during cutting. Finally, the ESI images were analyzed in parallel by EELS spectra.

For our investigation we chose the *R. pipiens* cutaneous pectoris, a very thin muscle that can be appropriately processed by quick-freezing, yielding high quality preparations of both fibers and synaptic terminals (31). We felt that muscle was a convenient model because its calcium distribution was already known better than in any other tissue. In particular, studies carried out by both ultrastructural (EPMA; immunocytochemistry) and cell fractionation techniques had revealed a differential distribution of calcium within the SR (1), with high accumulation at the level of terminal cisternae due to the clustering of the calcium binding protein, calsequestrin (41, 42). The available data on the protein calcium binding characteristics and on its degree of saturation indicate that in the calsequestrin-rich areas of the terminal cisternae, calcium levels around 80-100 mmol/liter are attained in resting muscles (43). The observation in our specimens of clearly appreciable EELS/ESI signals within terminal cisternae, on the one hand, strengthens the notion that no major relocation occurred within the SR during tissue processing; on the other hand, it suggests that calcium values around 100 mmol/liter can indeed be detected by the technique.

Compared to terminal cisternae, our findings on mitochondria appear open to questions. Previous EPMA observations in a variety of cell types revealed only moderate calcium contents most often around or below 1 mmol/liter (6, 13, 15, 17). In our preparations, numerous mitochondria failed to exhibit calcium signals, which is consistent with these previous studies, whereas others appeared positive, although to different extents. These signals could be regarded as a consequence of cell damage, which is similar to the calcium accumulation that occurs when isolated mitochondria are maintained under inappropriate conditions. However, EPMA showed that the elemental composition of the muscle fibers were not severely affected by our procedures. In addition, the calcium-rich mitochondria were localized in apposition to the triads, where extensive mitochondrial reuptake of the Ca^{2+} released from the SR could take place. Indeed, based on recent studies, mitochondria appear able to sense $[Ca^{2+}]_i$ variations in their microenvironment (4, 5, 44–47). Up until now, however, the molecular mechanisms of calcium binding (if any) to mitochondrial matrix components have not been investigated in detail and the relationship between free and total calcium is still undefined. Thus the significance of our ESI positive mitochondria is unclear and needs to be considered with great caution at the present time.

Within nerve terminals, calcium was high in some but not all endoplasmic reticulum cisternae, in apparent agreement with studies that predict its preferential accumulation in discrete regions (6, 48, 49). Synaptic vesicles are known to possess an efficient system of calcium uptake (50), yet the available data on their content are fragmentary and controversial (6, 25, 29).

Our results show relevant signals within the lumen of all vesicles, independent of their location with respect to the active zones.

In conclusion, the results reported here reveal that our quick-freezing ESI/EELS approach can be employed to map intracellular calcium with high spatial resolution and precise recognition, but only in intracellular organelles particularly rich in the element. Other advantages of the approach, not exploited in the present study but easy to predict, are the high temporal resolution typical of quick-freezing (msec) and the possible correlation with other techniques: cytosolic [Ca^{2+}] measurements (fluororescent dye imaging) and immunocytochemistry of Ca^{2+} binding proteins (immunogold labeling). By using these comprehensive studies, further biological and physiological information might become available soon in a variety of cellular systems.

We are indebted to Prof. A. Cantaboni and the staff of the Department of Pathology, S. Raffaele Hospital, for generously permitting our access to the Zeiss CEM 902 microscope. We are grateful to Dr. R. Door (Sektion Elektronenmikroskopie, University of Ulm) for very helpful suggestions and collaboration; and to Dr. M. Tonelli and P. L. Fabbri (University of Modena) for the EPMA analyses. We also thank Dr. C. Gambini for participating in the initial experiments and Ms. L. Di Giorgio for secretarial support. This work was supported by a research grant of the International Human Fronteer Science Program (to J.M.; Principle Investigator, Dr. Haruo Kasai).

1. Pozzan, T., Rizzuto, R., Volpe, P. & Meldolesi, J. (1994) *Physiol. Rev.* **74,** 595–636.
2. Grynkiewicz, G. M., Poenie, M. & Tsien, R. Y. (1985) *J. Biol. Chem.* **260,** 3440–3450.
3. Tsien, R. Y. (1989) *Methods Cell Biol.* **30,** 127–156.
4. Rizzuto, R., Simpson, W. P., Brini, M. & Pozzan, T. (1992) *Nature (London)* **358,** 325–327.
5. Rizzuto, R., Brini, M., Murgia, M. & Pozzan, T. (1993) *Science* **262,** 744–746.
6. Andrews, S. B. & Reese, T. (1986) *Ann. N.Y. Acad. Sci.* **483,** 284–294.
7. Hall, T. A. (1988) *Ultramicroscopy* **24,** 181–184.
8. LeFurgey, A., Bond, M. & Ingram, P. (1988) *Ultramicroscopy* **24,** 185–220.
9. Zierold, K. & Schäfer, D. (1988) *Scanning Microsc.* **2,** 1775–1779.
10. Nicaise, G., Gillot, I., Julliard, A. K., Keicher, E., Blaineau, S., Amsellem, J., Meyran, J. C., Hernandez-Nicaise, M., Ciapa, B. & Gleyzal, C. (1989) *Scanning Microsc.* **3,** 199–220.
11. Stelly, N., Halpern, S., Nicolas, G., Fragu, P. & Adoutte, A. (1995) *J. Cell Sci.* **108,** 1895–1919.
12. Shuman, H., Somlyo, A. V. & Somlyo, A. P. (1976) *Ultramicroscopy* **1,** 317–339.
13. Andrews, S. B., Leapman, R. D., Landis, D. M. D. & Reese, T. (1988) *Proc. Natl. Acad. Sci. USA* **85,** 1682–1685.
14. Somlyo, A. V., Gonzales-Serratos, H., Shuman, H., McClellan, G. & Somlyo, A. P. (1981) *J. Cell Biol.* **90,** 577–594.
15. Somlyo, A. P., Bond, M. & Somlyo, A. V. (1985) *Nature (London)* **314,** 622–625.
16. Somlyo, A. V., McClellan, G., Gonzales-Serratos, H. & Somlyo, A. P. (1985) *J. Biol. Chem.* **260,** 6801–6807.
17. Bond, M., Vadasz, G., Somlyo, A. V. & Somlyo, A. P. (1987) *J. Biol. Chem.* **262,** 15630–15636.
18. Baumann, O., Waltz, B., Somlyo, A. V. & Somlyo, A. P. (1991) *Proc. Natl. Acad. Sci. USA* **88,** 741–744.
19. Ottensmeyer, F. P. & Andrew, J. W. (1980) *J. Ultrastruct. Res.* **72,** 336–348.
20. Colliex, C. (1986) *Ann. N.Y Acad. Sci.* **483,** 311–325.
21. Shuman, H. & Somlyo, A. P. (1987) *Ultramicroscopy* **21,** 23–32.
22. Leapman, R. D. & Ornberg, R. L. (1988) *Ultramicroscopy* **24,** 251–268.
23. Wang, Y. Y., Ho, R., Shao, Z. & Somlyo, A. P. (1992) *Ultramicroscopy* **41,** 11–31.
24. Leapman, R. D., Hunt, J. A., Buchanan, R. A. & Andrews, S. B. (1993) *Ultramicroscopy* **49,** 225–234.
25. Probst, W. (1986) *Histochemistry* **85,** 231–239.
26. Poenie, M. & Epel, D. (1987) *J. Histochem. Cytochem.* **35,** 939–957.
27. Mentré, P. & Halpern, S. (1988) *J. Histochem. Cytochem.* **36,** 55–64.
28. Körtje, K. H. & Körtje, D. (1992) *J. Microsc. (Oxford)* **166,** 343–358.
29. Parducz, A. & Dunant, Y. (1993) *Neuroscience* **52,** 27–33.
30. Livesey, S. A., Del Campo, A. A., McDowall, A. W. & Stasny, J. T. (1991) *J. Microsc. (Oxford)* **161,** 205–215.
31. Torri Tarelli, F., Grohovaz, F., Fesce, R. & Ceccarelli, B. (1985) *J. Cell Biol.* **101,** 1386–1399.
32. Heuser, J. E. & Reese, T. S. (1981) *J. Cell Biol.* **88,** 564–580.
33. Porter, K. R. & Palade, G. E. (1957) *J. Biophys. Biochem. Cytol.* **3,** 269–300.
34. Peachey, L. D. (1965) *J. Cell Biol.* **25,** 209–231.
35. Roos, N. & Barnard, T. (1985) *Ultramicroscopy* **17,** 335–344.
36. Plattner, H. & Bachmann, L. (1982) *Int. Rev. Cytol.* **79,** 237–304.
37. Zierold, K. (1991) *J. Microsc. (Oxford)* **161,** 357–366.
38. Weibel, E. R. & Paumgartner, D. (1978) *J. Cell Biol.* **77,** 584–597.
39. Botton, G. & L'Espérance, G. (1992) *Ultramicroscopy* **41,** 287–290.
40. Door, R. & Gangler, D. (1995) *Ultramicroscopy* **58,** 197–210.
41. Jorgensen, A. O., Shen, A. C.-Y., Campbell, K. P. & MacLennan, D. H. (1983) *J. Cell Biol.* **97,** 1573–1581.
42. Franzini-Armstrong, C., Kenney, L. J. & Varriano-Marston, E. (1987) *J. Cell Biol.* **105,** 49–56.
43. Volpe, P. Simon, B. J. (1991) *FEBS Lett.* **278,** 274–278.
44. Rizzuto, R., Bastianutto, C., Brini, M., Murgia, M. & Pozzan, T. (1994) *J. Cell Biol.* **126,** 1183–1194.
45. Miller, R. J. (1991) *Prog. Neurobiol.* **37,** 255–285.
46. Martinez-Serrano, A. & Satrustegui, J. (1992) *Mol. Biol. Cell* **3,** 235–248.
47. Friel, D. D. & Tsien, R. W. (1994) *J. Neurosci.* **14,** 4007–4024.
48. Duce, I. R. & Keen, P. (1978) *Neuroscience* **3,** 837–848.
49. McGraw, C. F., Somlyo, A. V. & Blaustein, M. P. (1980) *J. Cell Biol.* **85,** 228–241.
50. Nicaise, G., Maggio, K., Thirion, S., Horoyan, M. & Keicher, E. (1992) *Biol. Cell.* **75,** 89–99.